Radiat Environ Biophys (2004) 43:77–84
DOI 10.1007/s00411-004-0238-7

ORIGINAL PAPER

Philipp Bernhardt · Werner Friedland · Herwig G. Paretzke

The role of atomic inner shell relaxations for photon-induced DNA damage

Received: 9 September 2003 / Accepted: 23 March 2004 / Published online: 2 July 2004

Abstract The influence of relaxations of atoms making up the DNA and atoms attached to it on radiation-induced cellular DNA damage by photons was studied by very detailed Monte Carlo track structure calculations, as an unusually high importance of inner shell ionizations for biological action was suspected from reports in the literature. For our calculations cross sections for photons and electrons for inner shell orbitals were newly derived and integrated into the biophysical track structure simulation programme PARTRAC. Both the local energy deposition in a small sphere around the interacting relaxed atom, and the number of relaxations per Gy and Gbp were calculated for several target geometries and many monoenergetic photon irradiations. Elements with the highest order number yielded the largest local energy deposition after interaction. The atomic relaxation after ionization of the L1 shell was found to be more biologically efficient than that of the K shell for high Z atoms. Generally, the number of inner shell relaxations produced by photon irradiation was small in comparison to the total number of double strand breaks generated by such radiation. Furthermore, the energy dependence of the total number of photon-induced and electron-induced relaxations at the DNA atoms does not agree with observed RBE values for different biological endpoints. This suggests that the influence of inner shell relaxations of DNA atoms on radiation-induced DNA damage is in general rather small.

Introduction

The relaxation of atoms excited by energy absorption from incident photon fields influences the biological damage caused by photon irradiation [1, 2, 3, 4, 5, 6, 7, 8, 9, 10, 11, 12, 13, 14, 15, 16]. After removal of inner shell electrons due to photoabsorption, the Compton effect, or by secondary electron interaction, the resulting hole is successively filled up by radiative and non-radiative transitions from outer shells whereby several low energy photons and electrons can be released. These emitted electrons have usually short ranges leading to a high local energy deposition on a nanometer scale, which is thought to be the size of the critical targets for many biological endpoints [17, 18, 19, 20, 21, 22]. These sizes were suggested by the high biological action effectiveness of C_K ultrasoft x-ray irradiation whose secondary electrons have only a range of approximately 7 nm in liquid water. Furthermore, the emission of many electrons leads to highly charged atoms that then gather electrons from the neighboring molecules, additionally increasing the complexity of the local molecular disturbance.

To test in a quantitative way whether these qualitative arguments in favor of high biological importance of inner shell ionization hold true, in this work both the number of ionizations and relaxations of DNA internal atoms and of attached atoms and their local energy deposition as a consequence of the emitted particle spectrum were quantified by the biophysical computer simulation package PARTRAC. The results were compared with observed values for the relative biological effectiveness of photons as a function of their energies for various endpoints to test the validity of published assumptions about the relevance of the relaxation effects.

Methods

The following description of methods used concentrates on the new cross sections for ionization of the inner shells by electrons and photons of DNA and DNA attached atoms in order to estimate the number and the intensity of electronic relaxations in the vicinity of the DNA in the cellular environment. All the other input data used in PARTRAC for a complete coupled photon and electron track structure simulation using structured targets are described in detail in [23].

P. Bernhardt · W. Friedland (✉) · H. G. Paretzke
GSF—National Research Center for Environment and Health,
Institute of Radiation Protection,
85764 Neuherberg, Germany
e-mail: friedland@gsf.de
Tel.: +49-89-31872767
Fax: +49-89-31873363

Table 1 Weight fractions of atoms in cellular plasma and DNA (%)

Element (Z)	Plasma	DNA
H (1)	10.9	3.5
C (6)	7.4	35.3
N (7)	2.5	15.9
O (8)	76.3	29.0
Na (11)	0.0	6.9
P (15)	2.6	9.4
S (16)	0.4	0.0

Table 2 Binding energy *B*, remaining nominal average charge of the relaxed DNA atom after inner shell ionization and average kinetic energy *U* of the inner shell electrons considered

Element (Z)	B (keV)	Charge	U (keV)
C-K (6)	0.29	2.0	0.43
N-K (7)	0.40	2.0	0.60
O-K (8)	0.54	2.0	0.79
Na-K (11)	1.06	2.4	1.52
P-K (15)	2.13	4.1	2.87
P-L1 (15)	0.19	3.0	0.44
P-L2 (15)	0.14	2.0	0.40
P-L3 (15)	0.14	2.0	0.40
Ca-K (20)	4.02	3.8	
Br-K (35)	13.44	7.2	
I-K (53)	33.16	11.0	
I-L1 (53)	5.16	12.5	
I-L2 (53)	4.86	10.7	
I-L3 (53)	4.55	10.3	
Pt-K (78)	78.62	11.1	
Pt-L1 (78)	13.86	15.3	
Pt-L2 (78)	13.31	11.4	
Pt-L3 (78)	11.57	11.1	

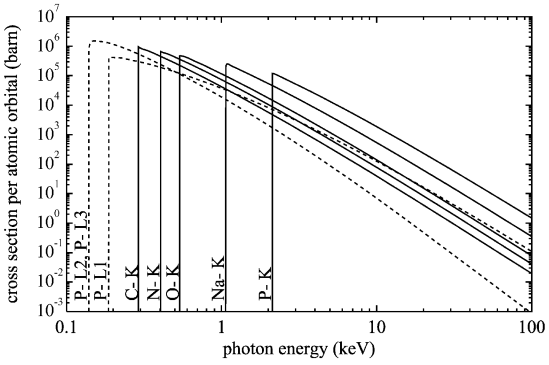

Fig. 1 Photoabsorption cross sections of the inner shells of the DNA atoms C, N, O, Na and P [24]. *Solid lines* K shells, *dashed lines* L shells

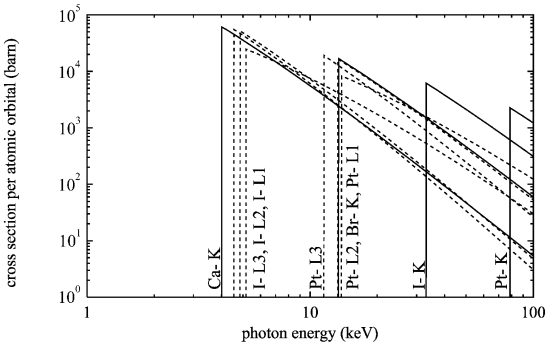

Fig. 2 Photoabsorption cross sections of the inner shells of the external elements Ca, Br, I and Pt [24]. *Solid lines* K shells, *dashed lines* L shells

Photon inner shell ionization cross section

Photons with energies between 0.1 keV and 1 MeV interact with matter via photoabsorption, coherent and incoherent scattering. Photoabsorption dominates in the low energy regime (up to a few 10 keV in low-Z materials) and mainly occurs at the inner shell electrons, which are almost not influenced by molecular binding. The photon cross sections for the inner shells are taken from the widely accepted atomic cross section database EPDL97 [24]. The binding energies used for the derivation of this database seem to differ from more recent values, as pointed out by the authors, but have the advantage of being consistent with their relaxation data EADL [25]. The absorption fine structure near to the binding energy edges is not incorporated in the data. The atomic weight fractions used for the DNA and the surrounding cellular plasma are given in Table 1. The values for the plasma are taken from [26], those for the DNA were derived from the atomic composition of a randomly chosen base sequence, including one sodium counter ion per nucleotide: 11.25 H, 9.75 C, 3.75 N, 6 O, 1 Na and 1 P.

Additionally, the ionization and relaxation effects of external high Z atoms attached to the DNA have been investigated. Such atoms can play an important role, e.g. in radiation research studies or in medical procedures. In principle, three ways of adding atoms to the DNA are possible: (i) external atoms or molecules can replace parts of the DNA, like the exchange of thymine bases by bromouracil or iodouracil [1, 4, 7, 8], (ii) charged external atoms or molecules like magnesium or calcium ions can replace the sodium counter ion [27, 28], or (iii) external molecules can be attached by hydrogen or covalent bonds, like cis platinum to the base guanine [29, 30]. In this work, inner shell ionization of calcium, bromine, iodine and platinum and subsequent relaxation is explored.

In Table 2 in the third column the binding energies of the inner shells of the DNA atoms and of the abovementioned external elements are listed. In Figs. 1 and 2 the inner shell photoabsorption cross sections that are mainly responsible for photon-induced relaxation in this energy range are given for the DNA and the external atoms. Whenever photon energy is sufficient for ionization of a shell, photon cross sections jump up immediately (resonance absorption). Afterwards the cross sections decrease about inversely to the power of 3 of photon energy, in contrast to a normal resonance behavior, because the ejected electron will take over the energy difference as its kinetic energy.

Electron inner shell ionization cross section

Electron ionization cross sections for the cellular plasma are taken from Dingfelder et al. [31] who derived cross sections for the model substance liquid water. For the DNA ionization cross sections have been calculated [32] with the help of the Relativistic Binary-Encounter-Bethe theory (RBEB) [33, 34]. According to the RBEB-formalism ionization cross sections σ per orbital for electron energies from the ionization threshold up to the relativistic region can be determined by:

$$\sigma = \frac{4\pi a_0^2 \alpha^4 N}{\left(\beta_t^2 + \beta_u^2 + \beta_b^2\right) 2b'} \left\{ \frac{1}{2} \left[\ln\left(\frac{\beta_t^2}{1-\beta_t^2}\right) - \beta_t^2 - \ln\left(2b'\right) \right] \left(1 - \frac{1}{t^2}\right) + 1 - \frac{1}{t} - \frac{\ln t}{t+1} \frac{1+2t'}{\left(1+t'/2\right)^2} + \frac{b'^2}{\left(1+t'/2\right)^2} \frac{t-1}{2} \right\},$$

where

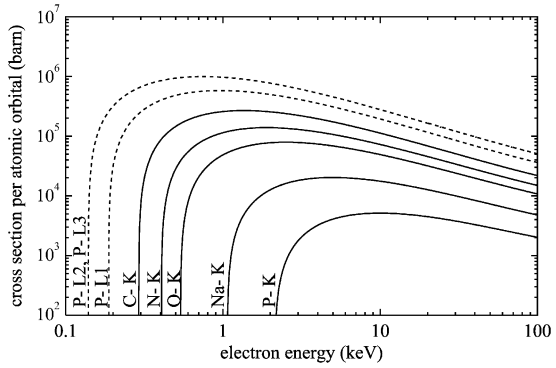

Fig. 3 Electron ionization cross sections of the inner shells of the DNA atoms C, N, O, Na and P. *Solid lines* K shells, *dashed lines* L shells

- a_0=Bohr radius (0.0529 nm)
- α=fine structure constant (0.007297)
- N=orbital electron occupation number
- T=kinetic energy of the incoming electron
- U=average kinetic energy of the bound target electron
- B=binding energy of the target electron
- t=T/B
- u=U/B
- m_ec^2=rest energy of the electron
- $t'=T/m_ec^2$
- $u'=U/m_ec^2$
- $b'=B/m_ec^2$
- $\beta_t^2=1-1/(1+t')^2$
- $\beta_u^2=1-1/(1+u')^2$
- $\beta_b^2=1-1/(1+b')^2$

For the determination of σ, specific values of B and U are necessary for every target orbital. Because B of the inner shells is quite independent of the molecular structure, it was directly taken from [24]. U can be computed by ab initio molecular orbital calculation. The results were obtained by using the Gaussian 98 system [35] and the spin restricted Hartree Fock method [36] with the 3-21G basis set [37] and are given in Table 2. Only values of the DNA subshells are presented because the probability for an electron to interact with the tightly bound inner shell orbitals of the external atoms is extremely small and was therefore neglected. In Fig. 3 the resulting electron ionization cross sections of the inner shells of the DNA atoms C, N, O, Na and P are presented. Interestingly, their total values are quite close to those of the photoabsorption cross sections. Nevertheless, these events occur rarely because of the large electron cross sections of the valence shells.

Relaxation after inner shell ionizations

Whenever an inner shell electron is removed by photoabsorption, the Compton effect or electron ionization, the atom relaxes by radiative (fluorescence) and non-radiative (Auger or Coster-Kronig) transitions. The emitted particle spectrum is calculated by a Monte Carlo atomic reorganization code following Pomplun et al. [38, 39], i.e. the holes are successively filled up by outer shell electrons until they have moved up to the valence shell. The transition probabilities and the emitted particle energies are taken from the EADL database [25], whereby the probabilities are scaled with the fraction of the number of the remaining electrons in a certain subshell and renormalized to 1. It is assumed that the angular distribution of the emitted particles is isotropic. Due to the condensed phase of a biological cell it is assumed that holes in the valence shells of its atoms are immediately filled up by electrons from neighboring molecules, i.e. valence orbitals are not depleted but have an unlimited electron reservoir (as compared to atoms in the gas phase). The difference between the binding energy of the initially released electron and the sum of the energies of all subsequently emitted particles is scored as a local energy deposition (in form of potential energy) at the location of the relaxed atom.

Cellular and DNA target model

The geometry of the DNA was defined by an atomic volume model [40, 41], i.e. with atomic spheres having radii scaled from their van der Waals radius which are then unified [23]. With this representation a piece of chromatin fiber with a stochastic cross linked architecture is generated, consisting of about 210,000 atoms. To simulate in the computer for the present purpose a human cell nucleus with 6 billion base pairs (6 Gbp) and 46 chromosomes in the stage of the interphase of the cell cycle, these chromatin pieces are lined up in a cylindric volume of 5 μm radius and 5 μm thickness submersed in cellular plasma. Thereby chromatin fiber loops and chromosome domains are considered. A complete description of this present DNA target modeling in PARTRAC can be found in [23, 42].

Calculations

In the simulation, the cell nucleus target model is irradiated with monochromatic photons that are homogeneously and isotropically distributed in space. A total energy of 50 MeV was deposited for each photon energy to achieve good statistics. The photon energies considered ranged from 0.1 keV to 1 MeV. To simulate charged particle equilibrium, all particle tracks which leave the cell nucleus are forced to reenter this area on the other side. Whenever particles interact inside the atomic volume of the DNA, the corresponding cross sections are applied, otherwise liquid water cross sections are used.

Results

The biological effectiveness of the relaxation cascades on the generation of DNA damage can be characterized, e.g. by two microdosimetric quantities: by the energy deposition density close to the relaxed atom, or by the number of inner shell ionizations produced per Gy and Gbp in dependence on the initial photon energy; the latter is further called number of relaxations per Gy and Gbp.

Relaxations of DNA atoms

In Fig. 4 the total energy deposition in a sphere around a relaxed DNA atom is given in dependence on the radius. The maximum distance was chosen as 5 nm because this is about the longest pathway which radiation-induced water radicals can travel to damage DNA assuming the cellular radical scavenging capacity [43]. The relaxation is initiated by a hole produced in a particular atomic subshell. The energy deposition at r=0 nm is equal to the amount of potential energy stored on average due to photon interaction after completion of the cascade. The P-K and P-L1 ionizations lead to the highest energy deposition within 5 nm. However, comparing the C-K, N-K and O-K relaxations, elements with lower Z values tend to generate higher local energy depositions in 5 nm spheres

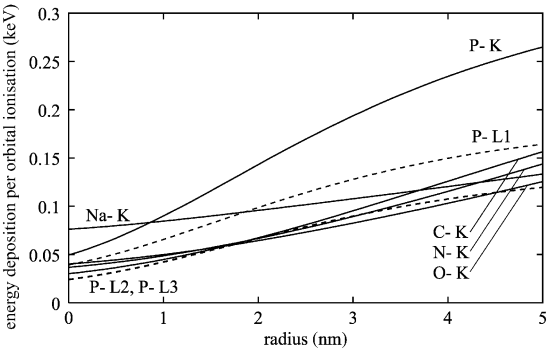

Fig. 4 Energy deposition per ionization of a certain atomic orbital in a sphere around the relaxed atom. *Solid line* K ionization, *dashed line* L ionization

around such events; as expected, P-L2 and P-L3 ionizations lead to similar energy deposition values.

Table 2 presents the nominal remaining average charge of the relaxed DNA atoms in the simulation cascade calculation after an inner shell ionization. Whereas C-K, N-K, O-K, P-L2 and P-L3 ionizations mostly lead to a single step relaxation cascade, holes in the Na-K, P-K and P-L1 subshells generate initially higher charged atoms. In the condensed phase, these charges are neutralized within far less than a nanosecond.

The numbers of relaxations per Gy and Gbp as a function of the photon energy in different DNA subshells are shown in Fig. 5. The total number is split up into the primary photon (photo effect, Compton scattering) and the secondary electron contributions of inner shell ionizations. Whereas the contribution of the photons strongly (about proportional to reciprocal photon energy) decreases for energies higher than the binding energy, the electron inner shell ionization contribution becomes more and more dominant, particularly for the low energy orbitals. In the case of Na-K and P-K ionizations, electron-induced relaxation could not be observed at all in the simulations.

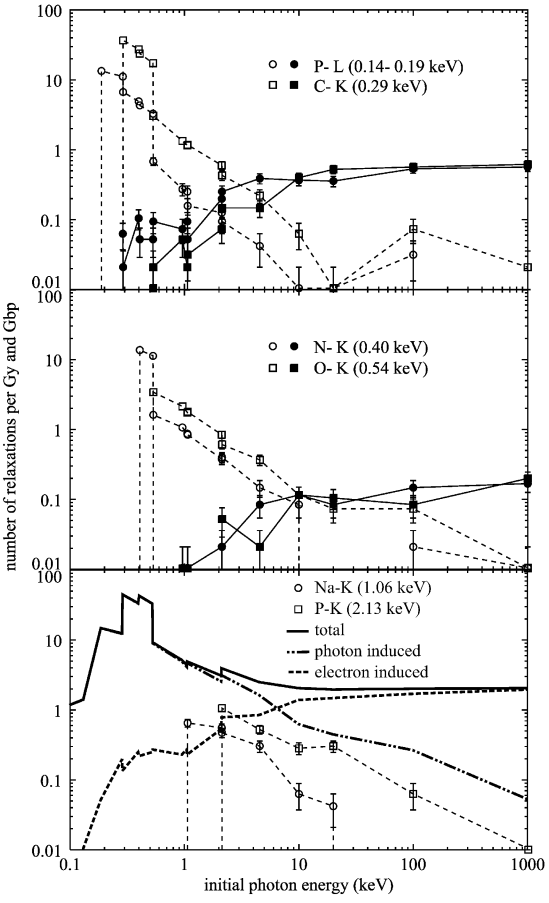

Fig. 5 Number of relaxations per Gy and Gbp initiated by ionizations of inner DNA orbitals as a function of energy of incident photons. *Open symbols* photon induced relaxations (photo effect, Compton scattering), *filled symbols* electron-induced relaxations (inner shell ionizations), *thick lines* total number for all atoms of the DNA (*solid*) with photon-induced part (*dash dot dot*) and electron induced part (*dashed*). Electron-induced relaxations after Na-K and P-K ionizations are below 0.01 per Gy and Gbp for all photon energies. *Bars* denote single standard deviations due to statistics

Relaxations of attached heavy atoms

The local energy deposition for inner shell relaxations of attached calcium, bromine, iodine and platinum atoms is given in Fig. 6, using the same procedure as in Fig. 4. Generally, atoms with larger Z-values, like iodine or platinum, tend to produce higher local energy deposition within spheres of 5 nm radius around such events. However, the L1 ionization of these atoms seems to generate higher energy depositions than a hole in the K shell. In particular the L1 shell ionization of platinum is very effective in provoking higher local energy densities.

In Table 2 the remaining nominal average charge of the relaxed external atom at early phases in the simulation after an inner shell ionization is given. In agreement with Fig. 6, the L1 shell ionizations of high Z atoms like I and Pt create initially higher charged atoms than the corresponding K ionization.

In the case of the DNA chloroterpyridine platinum complex a maximum concentration of 0.2 platinum atoms per nucleotide base pair can be achieved [14]. This leads to totally 1.2 billion attached atoms in a whole human cell nucleus.

Figure 7 shows calculated yields of inner shell photoabsorptions per Gy and 1 billion attached atoms. Yields derived from cross section data for the incident photon energies are represented by lines whereas symbols correspond to frequencies obtained in simulation calculations. Differences between these data sets are found above 15 keV due to contributions from secondary photons following Compton scattering processes. This dominating concurrence reduces the steep decrease of the relaxation cross section with increasing photon energy and suppresses the influence of the K edge of platinum. For each element the number of ionizations has been summed up for all subshells. Inner shell ionizations due to Compton effect and secondary electrons have been neglected; the

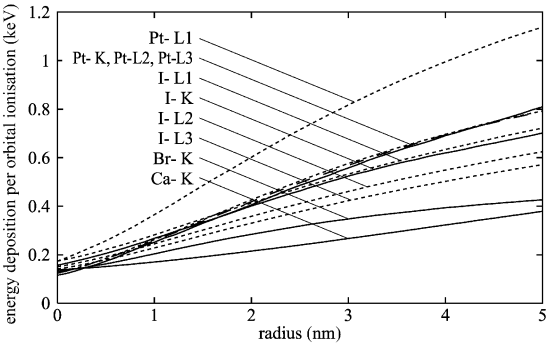

Fig. 6 Energy deposition due to and per inner shell ionization of a certain atomic orbital within a sphere around the relaxed atom in dependence on its radius. *Solid lines* K ionization, *dashed lines* L ionization

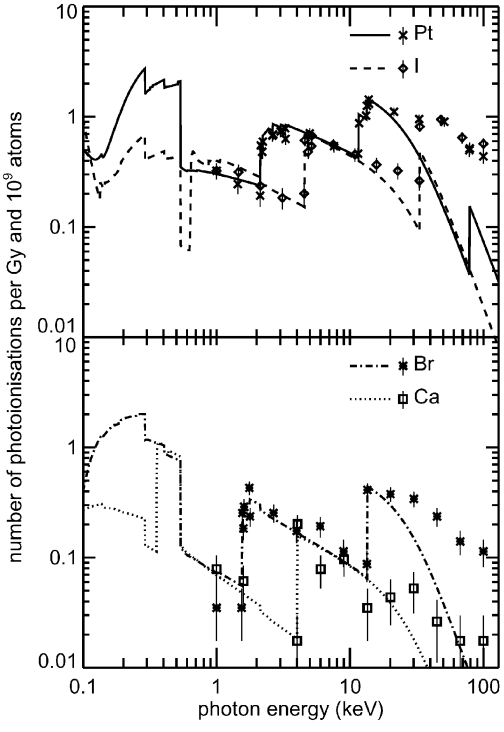

Fig. 7 Number of photoabsorptions per Gy and 10^9 attached atoms in dependence on the incident photon energy. *Lines* derived from cross sections, *symbols* simulation results, *bars* denote single standard deviations due to statistics

contributions of these effects are even smaller for the tightly bound subshells of the external atoms than for those of the DNA atoms shown in the previous chapter.

In comparison with the usual yields of double strand breaks (DSB) for x-ray irradiation of about 5–10 DSB/(Gy Gbp) [44] the number of relaxations of the attached atoms is quite small. The attachment of platinum is most efficient, for the maximum platinum concentration of 0.2 atoms per bp maxima of about 3 relaxations per Gy and Gbp occur between 0.25 and 0.55 keV and about 2 relaxations per Gy and Gbp are found for irradiation with photons of about 15 keV, slightly above the Pt-L1 absorption edge. The number of K shell ionizations of elements with high Z-values was found to be of only minor importance.

Discussion

The importance of inner shell ionizations of DNA atoms

Due to the increasing complexity of the relaxation pattern by emission of various photons and electrons, elements with higher order numbers tend to emit more low energy electrons. These, in turn, are then responsible for a high local energy deposition (Fig. 4). The relaxation pattern of ionized C-K, N-K and O-K shells mainly consists of a single step: a K-Lx-Ly Auger transition which emits one electron with energies of approximately 0.26 keV, 0.37 keV and 0.49 keV, respectively. The low energy and, therefore, the short range of the C-K Auger electron is responsible for the slightly higher local dose within 5 nm spheres. Since only one Auger electron is released per inner shell ionization, the local dose from the emitted photoelectron can become also important. If it has an energy similar to that of the Auger electron, the generated local dose can be even comparable to that of the P-K relaxation.

It should be mentioned that the additional damage by neutralization of the initially highly charged relaxed atom (Table 2) cannot yet be quantified with the present simulation code, nor can the Coulomb force effect of the increasing positive charge on the transport of these emitted slow electrons. The effectiveness of the neutralization could depend on the quantity of the remaining charge (see Table 2). The present calculation of the emitted particle spectra and the resulting positive charge is based on the single hole approach, neglects molecular binding effects, and uses a simplified description of the condensed phase. On the other hand, the lack of experimental values for processes in the condensed phase, particularly regarding the emission of low energy electrons, inhibits improvements [38, 39, 45]. Hence, it might be that the spectra determined here feature some errors which, however, should hardly influence the relative yields. In the case of the P-K ionization, the calculated emission of 4.1 electrons on average agrees well with results of other theoretical work [46, 47].

Figure 5 is useful to investigate the possible influence of inner shell ionizations and relaxations in the biological action of photons of different energies for different biological endpoints. The yields of photon-induced relaxations decrease with increasing photon energies because fewer and fewer photon absorption events are necessary to deposit a fixed amount of energy in a given volume. Despite the low probability of inner shell ionization by secondary electrons, the huge amount of secondary electrons produced by photon interactions leads to a slightly increasing yield of relaxations for subshells with binding energies below 1 keV for high initial photon energies.

The RBE values for different biological endpoints after photon irradiation in the energy range 0.1–1000 keV, like DSB production, cell survival, transformation and mutation, tend to increase slowly, when initial photon energy decreases [17, 18, 19, 20, 21, 22, 48, 49]. It reaches values of 2–4 (as compared to ^{60}Co-irradiation) for characteristic C_K irradiation of 0.28 keV which can only ionize outer shells and the phosphorus and sodium L shells. None of the investigated yields of ionizations of DNA subshells shows a behavior comparable to relevant RBE values. The photon-induced part decreases too rapidly, whereas the electron-induced part would lead to RBE values smaller than 1. The sum of both contributions is rather constant at higher photon energies but inflated by more than a factor of 10 between the C-K and the O-K shells. This observation is in agreement with the work of Goodhead et al. [50] who compared the number of relaxations for three initial characteristic photon energies with the corresponding RBE values for cell killing. For photon energies between 10 and 1000 keV, the total number of ionizations in atoms of the DNA due to photon plus electron-induced parts is almost constant whereas the measured induction of dicentrics decreases by a factor of 7 [51].

Furthermore, the total number of inner shell ionizations and subsequent relaxations is small in comparison with about 500 ionizations and excitations per Gy and Gbp in the DNA in all atomic shells. The decay of one incorporated ^{125}I atom generates about one DSB by the combination of the action of Auger electrons and of neutralization [52]. Assuming this value also for an inner shell vacancy relaxation of an atom within the DNA, the yield of DSBs per Gy and Gbp from this cause would be 40, 15, 3 and 1 for monoenergetic photons right at the C-K, N-K, O-K and P-K edge, respectively. However, such strong changes in the yields of DSBs per unit dose—in particular at the C-K and N-K edges—were not observed in such experiments when dry DNA plasmid films were irradiated above and below the absorption edges of C-K, N-K, O-K and P-K [5, 9, 11, 15]. Indeed, the energies required for a single as well as for a double strand break were constant at 388, 435 and 573 eV whereas the numbers of C-K, N-K and O-K shell ionizations were rather different at these three photon energies with the same attenuation inside the DNA sample [11]. The local DSB induction efficiencies of P-L, C-K and O-K shell ionizations were estimated as 0.12, 0.1 and 0.25 for photon energies of 250, 380 and 760 eV, respectively [15]; thus, a particular high intrinsic efficiency of C-K shell ionizations could not be deduced from the experiments. The sudden increase of the photon cross sections at the absorption edges, however, leads to an inhomogeneous dose distribution if DNA is dissolved and the ranges of all secondary electrons are rather small. The measured decrease of the cell survival by a factor of approximately 2 in cells at the C-K absorption edge [12, 15] can be fully explained by an accumulation of the dose in the vicinity of the DNA caused by the short range of 7 nm of the C-K Auger electrons [23, 47].

In conclusion, the different energy dependencies suggest that at least for photon energies above 1 keV relaxations, inner shell ionizations of atoms of the DNA are of minor importance for photon-induced radiation damage to DNA. This does not rule out that these events contribute for lower photon energies, in particular between the C-K and the O-K shell ionization energy, to a certain extent to the overall damage due to their comparatively high abundances.

Relaxation of attached atoms

The higher local dose around attached atoms in Fig. 6 is due to the more complex relaxation pattern. The dominance of the L1 subshells for elements with high order numbers is a consequence of the high fluorescence yield of the K shell of these atoms. K shell ionization causes mainly a radiative transition from the L2 and L3 shells, whereas the involvement of the L1 shell is excluded by the selection rules [53]. As photons do not contribute to the local dose close to their source, K shell ionization of platinum is comparable with respect to its microdosimetric consequences with L2 and L3 ionization. Generally, the amount of energy deposition in the local area around the absorption location is quite small. For example, the relaxation of a platinum K shell ionization emits particles (photons and electrons) with a total energy of about 78 keV, but only 0.8 keV, i.e. about 1% is absorbed within a sphere of 5 nm. The largest part of the initial relaxation energy is released during the first relaxation step, and even if this happens to be an Auger decay, the large mean free path for inelastic processes of this emitted electron dilutes any space correlation on a nanometric scale.

The amount of local energy deposition is, again, highly correlated with the nominally remaining positive charge of the relaxed atom (Table 2). It is not clear if these states exist at all in the condensed phase, because neutralization by fast electron transfer from neighboring molecules runs in parallel during the relaxation process and inhibits the build-up of strong electric fields [39].

Although the cross sections for photon inner shell ionizations of atoms with high Z-values are rather large, the event per se occurs quite rarely in comparison with the usual number of DSBs for low LET irradiation (Fig. 7). This is due to the small number of attached atoms per basepair. Furthermore, tightly bound orbitals like I-K or Pt-K require large photon energies for ionization and, therefore, the number of initially absorbed photons per unit dose is rather small. Irradiation with energies above the Pt-L1 subshell is most efficient since the L2 and L3 shells still contribute. The only small radiological effect of attaching high Z atoms to DNA has also been observed in experiments. In brominated yeast cells the yield of DSB per unit dose induced by x-rays above the Br-K absorption edge is increased by a factor of 1.3 [3], and cell survival is reduced by up to a factor of 1.2 [2]. The attachment of platinum to dry DNA plasmid films raised

the induced DSB level by a factor of 1.2 when the photon energy passes the Pt-L3 edge [13], and the attachment of calcium ions in dissolved DNA led to a DSB increase of 1.27 per unit dose at the Ca-K edge [10]. Assuming that a relaxation of such high Z atoms after an inner shell ionization leads to one DSB in the vicinity, the experimental data agree well with the relationship determined here, namely that above this edge approximately one relaxation per Gy and Gbp of an attached atom will increase the measured amount of usually 5–10 radiogenic DSB/(Gy Gbp) for low LET irradiation [44]. That explains why attaching of high Z atoms does not strongly increase the number of local DNA lesions per unit dose in irradiated cells.

Conclusions

In this work the contribution of inner shell ionizations and their relaxation in atoms of the DNA and in external atoms to radiation-induced DNA damage of photons in the cellular environment was investigated. As expected elements with large Z-values led to higher local energy deposition close to the relaxed atom. However, DNA atom relaxations do not seem to have a large influence on the radiation damage, because neither the shape of the energy dependence of the number of relaxations due to photon and electron inner shell ionization fits measured RBE values for different biological endpoints nor does the yield of DSB. Nevertheless, significant effects may occur due to the preferred localization of interactions of low energy photons at atoms of the DNA. Relaxations of the L1 shells of high Z elements attached to DNA seem to be more efficient than K shell ionization with respect to the number of emitted low energy electrons and the number of relaxations per unit dose.

Acknowledgments We thank Drs. Mitio Inokuti, Yong-Ki Kim and Michael Dingfelder for helpful discussions concerning the electron cross sections. This work is supported by the European Community under Contract No. FIGR-CT-2003-508842.

References

1. Maezawa H, Hieda K, Kobayashi K, Furusawa Y, Mori T, Suzuki K, Ito T (1988) Effects of monoenergetic X-rays with resonance energy of bromine K-absorption edge on bromouracil-labeled *E. coli* cells. Int J Radiat Biol Relat Stud Phys Chem Med 53:301-308
2. Usami N, Kobayashi K, Maezawa H, Hieda K, Ishizaka S (1991) Biological effects of Auger processes of bromine on yeast cells induced by monochromatic synchrotron X-rays. Int J Radiat Biol 60:757–768
3. Menke H, Kohnlein W, Joksch S, Halpern A (1991) Strand breaks in plasmid DNA, natural and brominated, by low-energy X-rays. Int J Radiat Biol 59:85–96
4. Furusawa Y, Maezawa H, Suzuki K, Yamamoto Y, Kobayashi K, Hieda K (1993) Uracil-DNA glycosylase produces excess lethal damage induced by an Auger cascade in BrdU-labeled bacteriophage T1. Int J Radiat Biol 64:157–164
5. Yamada H, Kobayashi K, Hieda K (1993) Effects of the K-shell X-ray absorption of phosphorus on the scission of the pentadeoxythymidylic acid. Int J Radiat Biol 63:151–159
6. Watanabe M, Suzuki M, Watanabe K, Suzuki K, Usami N, Yokoya A, Kobayashi K (1993) Mutagenic and transforming effects of soft-X-rays with resonance energy of phosphorus K-absorption edge. Int J Radiat Biol 61:161–168
7. Lawrence T, Davis MA, Normolle DP (1995) Effect of bromodeoxyuridine on radiation-induced DNA damage and repair based on DNA fragment size using pulsed-field gel electrophoresis. Radiat Res 144:282–287
8. Shinohara K, Nakano H, Ohara H (1996) Detection of Auger enhancement induced in HeLa cells labeled with iododeoxyuridine and irradiated with 150 kV X-rays—Effects of cysteamine and dimethylsulfoxide. Acta Oncol 35:869–875
9. Hieda K, Hirono T, Azami A et al. (1996) Single- and double-strand breaks in pBR322 plasmid DNA by monochromatic X-rays on and off the K-absorption peak of phosphorus. Int J Radiat Biol 70:437–445
10. Takakura K (1996) Double-strand breaks in DNA induced by the K-shell ionization of calcium atoms. Acta Oncol 35:883–888
11. Yokoya A, Watanabe R, Hara T (1999) Single- and double-strand breaks in solid pBR322 DNA induced by ultrasoft X-rays at photon energies of 388, 435 and 573 eV. J Radiat Res 40:145–158
12. Herve du Penhoat MA, Fayard B et al. (1999) Lethal effect of carbon K-shell photoionizations in Chinese hamster V79 cell nuclei: experimental method and theoretical analysis. Radiat Res 151:649–658
13. LeSech C, Takakura K, Saint-Marc C, Frohlich H, Charlier M, Usami N, Kobayashi K (2000) Strand break induction by photoabsorption in DNA-bound molecules. Radiat Res 153: 454–458
14. LeSech C, Takakura K, Saint-Marc C, Frohlich H, Charlier M, Usami N, Kobayashi K (2001) Enhanced strand break induction of DNA by resonant metal-innershell photoabsorption. Can J Physiol Pharmacol 79:196–200
15. Fayard B, Touati A, Herve du Penhoat MA et al. (2002) Cell inactivation and double-strand breaks: the role of core ionizations, as probed by ultrasoft X-rays. Radiat Res 157:128–140
16. Touati A, Herve du Penhoat MA, Fayard B et al. (2002) Biological effects induced by K photo-ionisation in and near constituent atoms of DNA. Radiat Prot Dosim 99:83–84
17. Goodhead DT, Thacker J, Cox R (1979) Effectiveness of 0.3 keV carbon ultrasoft X-rays for the inactivation and mutation of cultured mammalian cells. Int J Radiat Biol 36:101–114
18. Frankenberg D, Goodhead DT, Frankenberg-Schwager M, Harbich R, Bance DA, Wilkinson RE (1986) Effectiveness of 1.5 keV aluminum K and 0.3 keV carbon K characteristic X-rays at inducing DNA double-strand breaks in yeast cells. Int J Radiat Biol 50:727–741
19. Hill MA, Stevens DL, Stuart Townsend KM, Goodhead DT (2001) Comments on the recently reported low biological effectiveness of ultrasoft X-rays. Radiat Res 155:503–510
20. Frankenberg D, Kühn H, Frankenberg-Schwager M, Lenhard W, Beckonert S (1995) 0.3 keV Carbon K ultrasoft X-rays are four times more effective than γ-rays when inducing oncogenic cell transformation at low doses. Int J Radiat Biol 68:593–601
21. DeLara CM, Hill MA, Jenner TJ, Papworth D, O'Neill P (2001) Dependence of the yield of DNA double-strand breaks in Chinese hamster V79–4 cells on the photon energy of ultrasoft X-rays. Radiat Res 155:440–448
22. Thacker J,Wilkinson RE, Goodhead DT (1986) The induction of chromosome exchange aberrations by carbon ultrasoft X-rays in V79 hamster cells. Int J Radiat Biol 49:645–656
23. Bernhardt Ph, Friedland W, Jacob P, Paretzke HG (2003) Modeling of ultrasoft X-ray-induced damage using structured higher order DNA targets. Int J Mass Spectrom 223–224:579–597

24. Cullen DE, Hubbel JH, Kissel L (1997) EPDL97 The evaluated data library, '97 Version. Lawrence Livermore National Laboratory, UCRL-ID-50400 6
25. Perkins ST, Cullen DE, Chen MH, Hubbel JH, Rathkopf R, Scofield J (1991) Tables and graphs of atomic subshell and relaxation data derived from the LLNL evaluated atomic data library (EADL), Z=1–100. Lawrence Livermore National Laboratory. UCRL-50400 30
26. ICRU (1989) Tissue substitutes in radiation dosimetry and measurement. Report 44. International Commission on Radiation Units and Measurements, Bethesda, MD
27. Chiu TK, Dickerson RE (2000) 1 Å crystal structures of B-DNA reveal sequence-specific binding and groove-specific bending of DNA by magnesium and calcium. J Mol Biol 301:915–945
28. Yuan H, Quintana J, Dickerson RE (1992) Alternative structures for alternating poly(dA-dT) tracts: the structure of the B-DNA decamer C-G-A-T-A-T-A-T-C-G. Biochemistry 31:8009–8021
29. Wing RM, Pjura P, Drew HR, Dickerson RE (1984) The primary mode of binding of cisplatin to a B-DNA dodecamer: C-G-C-G-A-A-T-T-C-G-C-G. EMBO J 3:1201–1206
30. Coste F, Malinge JM, Serre L, Shepard W, Roth M, Leng M, Zelwer C (1999) Crystal structure of a double-stranded DNA containing a cisplatin interstrand cross-link at 1.63 Å resolution: hydration at the platinated site. Nucleic Acids Res 27: 1837–1846
31. Dingfelder M, Hantke D, Inokuti M, Paretzke HG (1998) Electron inelastic scattering cross sections in liquid water. Radiat Phys Chem 53:1–18
32. Bernhardt Ph, Paretzke HG (2003) Calculation of electron impact ionization cross sections of DNA using the Deutsch-Mark and Binary-Encounter-Bethe formalisms. Int J Mass Spectrom 223–224:599–611
33. Kim YK, Rudd ME (1994) Binary-encounter-dipole model for electron-impact ionization. Phys Rev A50:3954–3967
34. Kim YK, Santos JP, Parente F (2000) Extension of the binary-encounter-dipole model to relativistic incident electrons. Phys Rev A62:052710
35. Frisch Æ, Frisch MJ (1998) Gaussian 98 user's reference. Gaussian, Pittsburgh
36. Binkley JS, Pople JA, Dobosh PA (1974) The calculation of spin-restricted single-determinant wavefunctions. Mol Phys 28:1423–1429
37. Binkley JS, Pople JA, Hehre WJ (1980) Self-consistent molecular orbital methods. XXI. Small split-valence basis sets for first-row elements. J Am Chem Soc 102:939–947
38. Pomplun E, Booz J, Charlton DE (1987) A Monte Carlo simulation of Auger cascades. Radiat Res 111:533–552
39. Pomplun E (2000) Auger electron spectra. Acta Oncol 39:673–679
40. Pomplun E (1991) A new DNA target model for track structure calculations and its first application to I-125 Auger electrons. Int J Radiat Biol 59:625–642
41. Michalik V, Begusova M (1994) Target model of nucleosome particle for track structure calculations and DNA damage modelling. Int J Radiat Biol 66:267–277
42. Friedland W, Jacob P, Paretzke HP, Merzagora M, Ottolenghi A (1999) Simulation of DNA fragments distributions after irradiation with photons. Radiat Environ Biophys 38:39–47
43. Roots R, Okada S (1975) Estimation of life times and diffusion distances of radicals involved in X-ray-induced DNA strand breaks or killing of mammalian cells. Radiat Res 64:306–320
44. Prise KM, Ahnström G, Belli M et al. (1998) A review of DSB induction data for varying quality radiations. Int J Radiat Biol 74:173–184
45. Charlton DE, Booz J (1981) A Monte Carlo treatment of the decay of ^{125}I. Radiat Res 87:10–23
46. Humm JL (1984) The analysis of Auger electrons released following the decay of radioisotopes and photoelectric interactions and their contribution to energy deposition. KFA Report JUL-1932, pp 100–109
47. Terrissol M, Vrigneaud JM (2001) Modelling ultrasoft X-rays effects on DNA. Proceedings of Lisbon MC 2000 Conference, Springer
48. Prise KM, Folkhard M, Davies S, Michael BD (1989) Measurements of DNA damage and cell killing in Chinese hamster V79 cells irradiated with aluminum characteristic ultrasoft X-rays. Radiat Res 117:489–499
49. Hill MA, Veccia MD, Townsend KMS, Goodhead DT (1998) Production and dosimetry of copper L ultrasoft X-rays for biological and biochemical investigations. Phys Med Biol 43:351–363
50. Goodhead DT, Thacker J, Cox R (1981) Is selective absorption of ultrasoft x-rays biologically important in mammalian cells? Phys Med Biol 26:1115–1127
51. Schmid E, Regulla D, Kramer H-M, Harder D (2002) The effect of 29 kV X-rays on the dose response of chromosome aberrations in human lymphocytes. Radiat Res 158:771–777
52. Krisch RE, Sauri CJ (1975) Further studies of DNA damage and lethality from the decay of iodine-125 in bacteriophages. Int J Radiat Biol 27:553–560
53. Landau LD, Lifshitz EM (1985) Quantum mechanics. Pergamon Press, Oxford